Small Strain Mechanical Properties of Latex-Based Nanocomposite Films

Christopher J.G. Plummer,[1] *Riccardo Ruggerone,*[1] *N. Negrete-Herrera,*[2] *Elodie Bourgeat-Lami,*[2] *Jan-Anders E. Månson**[1]

Summary: A waterborne latex-based technique, in which functionalized laponite is attached to PS and acrylic latex particles, is used to prepare films containing up to 50 wt% laponite. At high laponite contents this leads to a cellular arrangement of the laponite-rich layers, concentrated at the latex particle interfaces. MDSC shows that a significant proportion of the organic matrix does not contribute to the glass transition. However, this ''rigid'' matrix fraction arises from intercalation of the laponite stacks, and cannot account for the large increases in global stiffness in the rubbery state ($T > T_g$) on laponite addition. The mechanical response for $T > T_g$ is therefore discussed in terms of a four-phase structure, in which the intercalated laponite stacks embedded in a matrix with a relatively high rubbery modulus form a cellular structure, which is in turn embedded in a matrix whose modulus is closer to that of the bulk polymer. The importance of the cellular arrangement is underlined by the much lower rubbery modulus observed by DMA in specimens produced by deforming the original films in plane strain compression to produce oriented textures with relatively little connectivity between the laponite-rich layers.

Keywords: differential scanning calorimetry (DSC); electron microscopy; emulsion polymerization; mechanical properties; nanocomposites

Introduction

Clay based nanocomposites have provoked wide interest since the discovery of significant property improvements in polyamides containing low concentrations of exfoliated clay platelets.[1] Classical scale-independent models for particle reinforcement predict the very high aspect ratios of such platelets to result in greater tensile stiffness than for equiaxed particles, particularly if the platelets are aligned with the tensile axis.[2,3] Moreover, the reduced dimensions of the platelets (thickness of about 1 nm), and hence the large interfacial area per unit volume, imply that local changes in the matrix properties associated with the platelet-matrix interface may also significantly modify global properties.[4–8] However, these factors may also result in large increases in melt viscosity, so that processing requirements often place limits on clay contents at high degrees of exfoliation.[9] In latex-based technologies for film formation, on the other hand, processing characteristics depend primarily on the carrier fluid, the solids content of the latex and the presence of processing additives, so that if particles can be pre-formed with high clay contents, the ''viscosity problem'' associated with melt processing need not arise. Encapsulation of clay particles remains challenging, but an alternative is to introduce the clay into the carrier fluid and/or attach clay platelets to the latex

[1] Laboratoire de technologie des composites et polymères (LTC), Ecole Polytechnique Fédérale de Lausanne (EPFL), CH-1015 Lausanne, Switzerland
Fax: (+41) 021 693 5880;
E-mail: jan-anders.manson@epfl.ch
[2] Chimie, Catalyse, Polymère, Procédé, C2P2/LCPP, UMR 5265 CNRS/CPE/UCBL, Bât. 308F, BP 2077-43, Bd. Du 11 Nov. 1918, 69616 Villeurbanne Cedex, France

particle surfaces to give an ''armored'' particle morphology. If the latex particles are small, a high degree of dispersion of the clay may thus be maintained on drying, even at high clay contents. In what follows, a macromonomer has been used to promote interactions between atactic polystyrene (PS) and poly(methyl methacrylate-*co*-butylacrylate) (henceforth referred to as ''acrylate'') latexes and synthetic laponite clay during emulsion polymerization, so that the laponite adheres strongly to the latex particle surfaces.[10–12] Because the T_g of the PS/laponite latexes is well above room temperature, film formation requires sintering at high *T*. Hence, whilst the focus of the discussion will be on the PS/laponite films, an effort has also been made to assess the extent to which the behavior of this model system is reflected by that of systems such as the low T_g acrylic/laponite latexes considered here, whose characteristics are closer to those of latexes currently used in coatings applications.

Experimental Part

The required quantity of laponite (Laponite RD (Rockwood Additives)) was dispersed in water with a peptizing agent (sodium pyrophosphate (Aldrich), 10% by weight of laponite) and a surfactant (sodium dodecyl sulphate (SDS) (Acros Organics), 5% by weight of laponite) and stirred for 1 to 2 hours. 5% macromonomer (poly(ethylene oxide) 1000 monomethyl ether methacrylate (Polysciences)) by weight of laponite was then added to functionalize the hydrophilic laponite surface and promote attachment of the laponite to the polymer particles. The functionalized laponite suspension was introduced into a reactor and stirred under a nitrogen atmosphere. After degassing, the monomer (200 g/L of styrene, (Aldrich) or a 1:1 mixture by weight of methyl methacrylate (MA) and butyl acrylate (BA) (Aldrich)) and the initiator (2,2′ azobis-(cyanopentanoic acid) (Wako Chemicals), 0.5% with respect to the monomer) were added to the suspension, and polymerization allowed to proceed at 70 °C for 4 hours. The characteristics of the latexes are summarized in Tables 1 and 2. When referring to the latexes, use will be made of the nominal clay contents in these tables, although this may differ from the content of the films determined by ashing, also be referred to in what follows. The particle diameters were also measured by scanning and transmission electron microscopy (SEM and TEM), giving values of approximately 80 nm for both latexes, and the relatively large values from dynamic light scattering (DLS) were attributed primarily to particle agglomeration. Consolidated PS/laponite films were prepared from the corresponding latexes by drying and sintering for 20 min at 160 °C under a force of 3 to 50 kN (Fontijne Holland Press), depending on the laponite content, to give transparent films of about 0.3 mm in thickness. The acrylic nanocomposite films were prepared using the same technique, but at 100 °C. The distribution of

Table 1.
Characteristics of the PS/laponite latexes.

Initial (nominal) laponite content with respect to monomer [wt%]	DLS Particle diameter [nm]	SDS content [g/L]	Solids content [%]	Conversion [%]
0	82	2	16.6	97.8
2.5	93	2	17.2	99.4
5	86	2	17.5	99.2
7.5	90.1	2	17.8	97.9
10	78	2	17.5	94.1
20	72	2	18.1	89.1
30	167.7	2	20.4	97.4
50	193	2	23.0	93.5

Table 2.
Characteristics of the acrylate/laponite latexes.

Initial (nominal) laponite content with respect to monomer [wt%]	Particle diameter from DLS [nm]	SDS content [g/L]	Solids content [%]	Conversion [%]
0	83	2	16.2	99
10	> 1 μm	2	16.6	89
20	> 1 μm	2	19.4	97
30	> 1 μm	2	20.4	98
50	> 1 μm	2	20.2	100

the laponite platelets was investigated by embedding the latex in a water soluble melamine-based resin (Nanoplast FB 101 kit, Polysciences Inc.), sectioning with an ultramicrotome (Reichert-Jung Ultracut E) equipped with a diamond knife (Diatome) and observed using a Philips CM20 TEM at 200 kV. The consolidated film morphologies were investigated by TEM of thin microtomed sections prepared directly from the films. Dynamic mechanical analysis (DMA) temperature scans were carried out at 10 K/min and 1 Hz in the range 25 to 160 °C for the PS and −50 to 150 °C for the acrylic nanocomposites, using $10 \times 20 \times 0.3\,mm^3$ strips cut from the consolidated films (10 measurements per system). Modulated differential scanning calorimetry (MDSC) (TA instruments Q100, calibrated with sapphire standards) was used to measure the glass transition temperature, T_g, and reversing heat capacity, C_p, as a function of T (5 K/min heating scans, modulation signal ± 0.5 K, period 100 s).

Results and Discussion

Figure 1 shows acrylic latex particles synthesized with 10 wt% laponite embedded in melamine. Laponite was visible at the particle surfaces, although it also remained dispersed in the original aqueous phase. Both the PS/laponite films, whose microstructure has been described in detail elsewhere,[10,13] and the acrylic/laponite films showed a cellular microstructure at high laponite contents (Figure 2), owing to accumulation of the laponite at the original particle boundaries, in the form of stacks of platelets with a well-defined platelet separation, as evidenced by both TEM and wide angle X-ray scattering (WAXS). The diameters of the cells formed by the laponite-rich regions were consistent with the latex particle diameters of about 80 nm. The storage modulus and α transition temperature, T_α, taken to correspond to the peak in the loss factor (tan δ), generally showed a weak increase with increasing laponite content in the glassy state (Figures 3 and 4), with the exception of the PS/5 wt% laponite films, whose modulus was greater than for 10 and 20 wt% laponite, and whose T_α and T_g were also relatively high. This was attributed to a higher degree of exfoliation and dispersion at 5 wt% laponite. Moreover, the overall trends in the mechanical reinforcement below T_α could be accounted for using

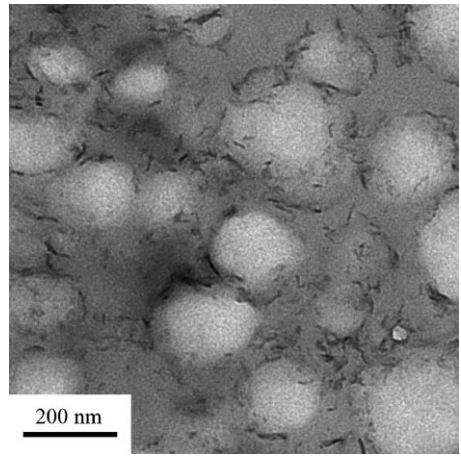

Figure 1.
TEM micrograph of a thin section from an acrylic/10 wt% laponite latex embedded in melamine-formaldehyde and sectioned at room temperature.

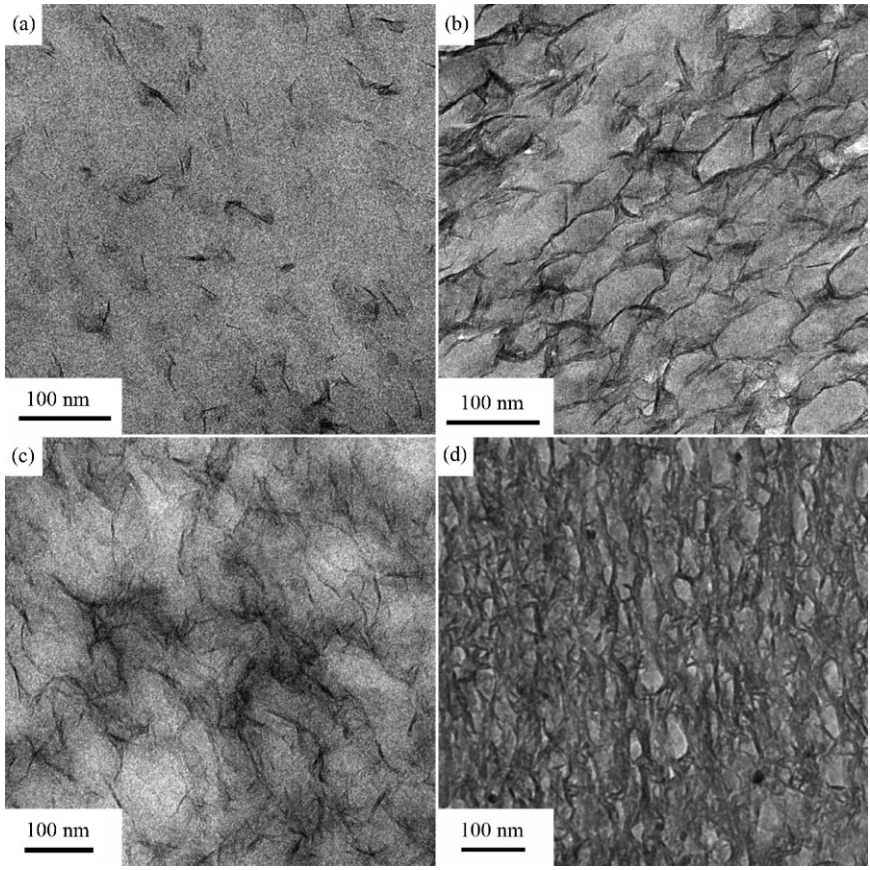

Figure 2.
TEM images of microtomed thin sections from consolidated nanocomposites prepared from (a) PS/5 wt% laponite, (b) PS/50 wt% laponite, (c) acrylate/10 wt% laponite, (d) acrylate/50 wt% laponite.

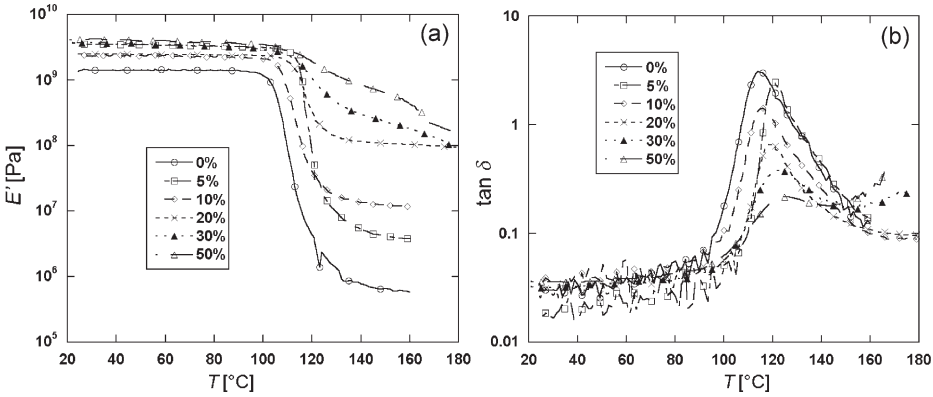

Figure 3.
DMA cans for PS/laponite nanocomposites for the different nominal laponite contents indicated: (a) the storage modulus (E') and (b) the loss factor (tan δ).

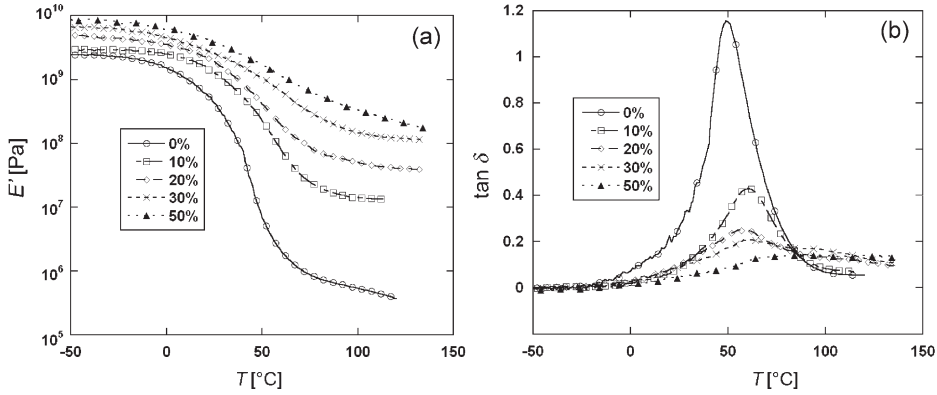

Figure 4.
DMA scans for acrylic/laponite nanocomposites for the different nominal laponite contents indicated: (a) the storage modulus (E') and (b) the loss factor (tan δ).

classical models for particle reinforcement and the laponite particle dimensions estimated from TEM micrographs.[10,13] Above T_α, on the other hand, the mechanical reinforcement was much greater than predicted by such models. Moreover, at the highest laponite contents (30 and 50 wt%), there was no clearly defined rubbery plateau (Figures 3a and 4a), and a suggestion of a second peak in the loss factor (Figures 3b and 4b), particularly for the PS/laponite films, although no corresponding transition was detected by MDSC.

Figure 5 shows MDSC reversing heat flow curves in the region of T_g normalized with respect to the mass of the organic part of the film in each case, determined by ashing, which was generally lower than the nominal laponite contents given in Tables 1 and 2. The step in heat capacity ΔC_p corresponding to T_g diminished significantly with increasing laponite content in both the PS and acrylate films. Changes in ΔC_p may be interpreted directly in terms of the proportion of the matrix that contributes to the glass transition, particularly since the absolute values of C_p varied little with laponite content below T_g. This leads to the idea of a ''rigid amorphous fraction'' (RAF), originally advanced to account for the behavior of semicrystalline polymers,

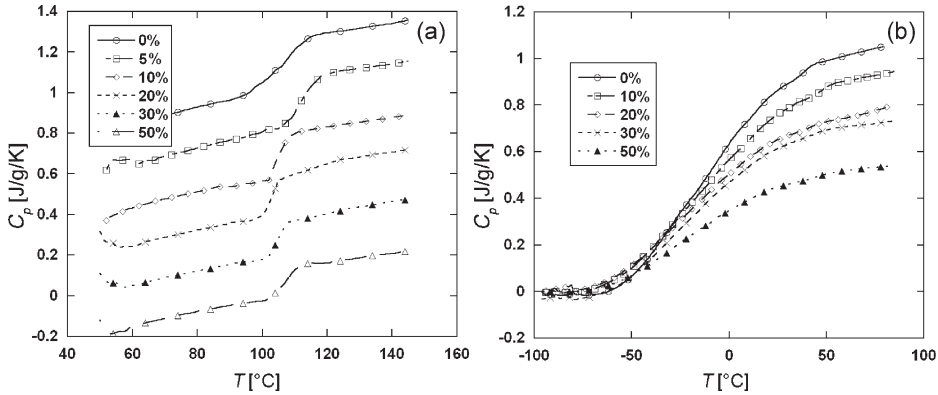

Figure 5.
Results from MDSC temperature scans for (a) PS/laponite nanocomposites and (b) acrylic/laponite nanocomposites containing different nominal weight percentages of laponite as indicated. The curves in (a) have been displaced vertically for clarity.

and which may be defined as

$$\phi_{RAF} = 1 - \frac{\Delta C_p}{\Delta C_{p,pure}} \quad (1)$$

where the subscript *pure* refers to ΔC_p for the unmodified matrix.[14,15] In the case of the acrylate, the choice of step height was somewhat ambiguous. A well defined step in C_p was visible in the range of T corresponding to the α transition, but it was superposed onto a broader transition spanning about 100 K. This was attributed to segregation of the comonomers owing to their differing reactivities,[16] and comparison of the derivatives of the heat flow curves suggested this effect not to depend on the laponite content. Indeed, similar values were obtained from equation (1) for ϕ_{RAF} in this case, regardless of whether the whole transition was used to define ΔC_p or just the step associated with the α transition.

ϕ_{RAF} is given as a function of the laponite content of the films determined by ashing in Figure 6 for the PS and acrylic films, showing a nearly linear dependence. Given a density of 2.53 gcm^{-3} for laponite, 45 wt% corresponds to a laponite volume fraction, ϕ_L, of about 25%. From WAXS, the (001) spacing of the intercalated laponite stacks in the laponite-rich regions in the PS/laponite films was 1.48 nm, regardless of composition, which compares with a spacing of 1 nm in the absence of intercalation. The volume of intercalated material therefore represented about 10% of the total volume of organic material, in good agreement with ϕ_{RAF} determined by MDSC. In the acrylates the (001) spacing determined by WAXS was about 2 nm for all the compositions studied, from which it was concluded that ϕ_{RAF} reflected immobilization of all the intercalated material in PS/laponite, whereas a proportion of the intercalated material retained some mobility in acrylate/laponite (although the overall degree of immobilization was similar in the two systems).

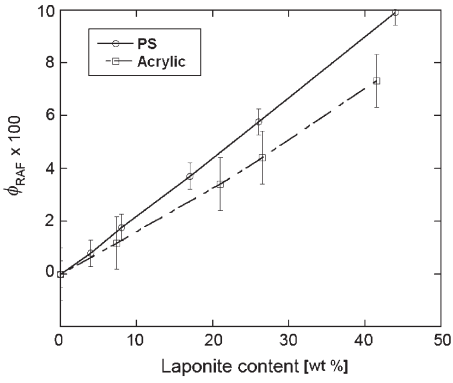

Figure 6.
ϕ_{RAF} for PS/laponite and acrylic/laponite nanocomposites as a function of the laponite content measured by ashing.

These results suggest that the PS/laponite nanocomposites in the rubbery state might be modeled as a rubbery continuum containing intercalated laponite stacks, whose organic content is glassy. Given a modulus of 178 GPa for the laponite platelets, and a modulus for the intercalated material of about 2 GPa, the in-plane modulus of the stacks, E_f, is estimated from simple mixing rules to be close to 120 GPa, i.e. very much greater than the matrix modulus, E_m, of 0.8 MPa for PS in the rubbery plateau region (Figure 3(a)). In the classical Halpin-Tsai framework, and for $E_f \gg E_m$, the tensile modulus, E, of a composite containing such stacks aligned with the tensile axis is approximately[2]

$$E \approx \frac{1 + 2\alpha\phi}{1 - \phi} E_m \quad (2)$$

where α is the aspect ratio and $\phi = 1.48\phi_L$ is the volume fraction occupied by the laponite stacks. In the PS/20 wt% laponite films, for example, the stack aspect ratio observed by TEM was 5.5. The laponite content from ashing was 18 wt% and ϕ was about 12%. E is therefore estimated from Equation 2 to be 2.1 MPa, which is orders of magnitude lower than the observed plateau modulus of about 100 MPa (indeed, the calculated E is an overestimate owing to a lack of preferential orientation of the stacks in the cellular morphology, although this may be offset by the large strain mismatch between the soft matrix and the rigid filler, which would tend to reduce the reinforcing effect of this latter).

Equation (2) has been plotted in Figure 7 as a function of ϕ_L or $\alpha = 5.5$

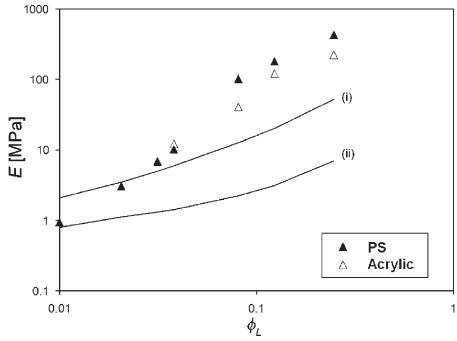

Figure 7.
E in PS/laponite and acrylic/laponite films at 160 and 100 °C respectively as a function of ϕ_L, along with predictions from equation (2) for (i) $\alpha = 54$ and (ii) $\alpha = 5.5$.

(value for PS stacks at high laponite contents) and 54 (the observed mean aspect ratio of a single laponite platelet[10]) and $E_m = 0.8$ MPa, which represent the limiting cases for the PS/laponite. Also given are data for the rubbery modulus of the PS/laponite (160 °C) and acrylic/laponite (120 °C) nanocomposite films, showing equation (2) not only to fail to account quantitatively for the data at relatively large ϕ_L, but also suggesting a significantly stronger increase in E with ϕ_L at low laponite contents than the nearly linear dependence implied by equation (2). Similar results have been obtained using other mechanical models based on the assumption of independent particles and $E_m = 0.8$ MPa so that these assumptions must clearly be questioned in the present context.[10] As a starting point for an improved description of the elastic response of the films above T_g, the laponite-rich regions have been modeled as an isotropic three-dimensional cellular foam network with a cell diameter of the order of the latex particle diameter. For a thin-walled foam embedded in a soft matrix, the tensile modulus in the rubbery state[17,18]

$$E = \left(1 - \frac{\rho}{\rho_s}\right) E_m + C\left(\frac{\rho}{\rho_s}\right)^n E_w \approx C\left(\frac{\rho}{\rho_s}\right)^n E_w \quad (3)$$

if $E \gg E_m$, where ρ is the foam density (excluding the matrix), ρ_s is the cell wall density and E_w is the cell wall modulus (generally assumed to be isotropic), C is a constant, generally of the order of or less than unity, and the exponent n depends on the geometry of the foam and the deformation mode. The modulus of both a monodisperse closed cell structure and an incompressible open cell structure, in which tensile deformation of cell walls dominates, is predicted to depend linearly on ρ/ρ_s, whereas n is expected to be close to 2 for a monodisperse open cell structure in which bending deformation dominates, although these exponents may be modified in the presence of a distribution of cell sizes and in the case of mixed closed/open cell structures.[17]

In order to test whether connectivity in the cellular arrangement of the laponite-rich regions plays an important role in the mechanical response, the films were deformed in plane strain compression (at 160 and 140 °C for the PS and the acrylates respectively) in order to break up the cellular structure, giving microstructures such as that shown in Figure 8(b). As seen in Figure 8(a), in the case of PS/20 wt% laponite films, plane strain compression resulted in a decrease in the rubbery modulus by about an order of magnitude, although the glassy modulus and T_α both showed a slight increase. Similar results were obtained for acrylate/20 wt% laponite films (it was not possible to extend this approach to higher laponite contents owing to the increasing brittleness and flow resistance of the nanocomposites). The trends in glassy modulus and T_α may be accounted for by the increased orientation and dispersion of the laponite stacks after compression. However the large decrease in rubbery modulus strongly suggests the initial cellular arrangement to be an important factor in the mechanical response at temperatures above T_g. The poorly defined rubbery plateaus in Figures 3(a) and 4(a) and the suggestion of a second relaxation peak (particularly in Figure 3(b)) also point to the importance of

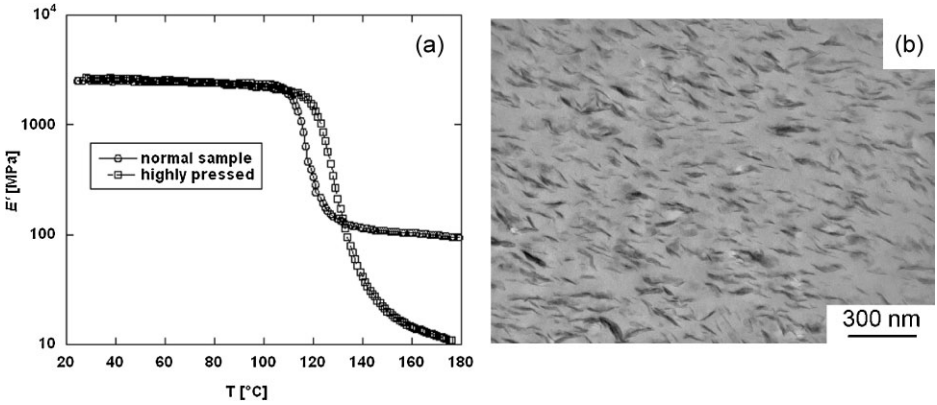

Figure 8.
(a) E' as a function of T from DMA scans on PS/20 wt% laponite films before and after plane strain compression; (b) TEM micrograph of a thin section from a PS/20 wt% laponite film after plane strain compression.

the cellular structure, since break-up is also expected to occur during the DMA measurements owing to poor strain control at the highest temperatures, leading to a decrease in E' and accounting for the observation that the apparent relaxation peak is not reflected by DSC (so that it cannot be interpreted in terms of a distinct T_g associated with confined matrix material, for example).

TEM measurements on PS/laponite indicate the average laponite stack thicknesses initially to increase with increasing laponite content (2.5, 8.4 and 9.9 nm for nominal laponite contents of 5, 10 and 20 wt% respectively, i.e. $\alpha. = 22, 6.4$ and 5.5, but to level off at approximately 10 nm ($\alpha. = 5.4$) at the highest nominal laponite contents (20 to 50 wt%).[10] If the effective cell wall thickness is taken somewhat arbitrarily to equal twice the stack thickness, the mean laponite concentration in a continuous closed-cell structure with spherical cells is predicted to increase from 20 to about 57% by volume as the nominal overall laponite content increases from 20 to 50 wt%, but to remain at between roughly 10 and 20% by volume at lower overall concentrations. Based on these estimates for the wall thicknesses and hence the local laponite concentration, the laponite particle aspect ratios, and the estimated laponite stack modulus of 120 GPa, equation (2) may be used to calculate an in-plane wall modulus, E_w. E_w may then be combined with equation (3) to give

$$E = \left(1-\frac{\rho}{\rho_s}\right)E_m + C\left(\frac{\rho}{\rho_s}\right)^n E_w = \left(1-\frac{\rho}{\rho_s}\right)E_m + C\frac{1+2\frac{\rho_s}{\rho}\alpha\phi}{1-\frac{\rho_s}{\rho}\phi}\left(\frac{\rho}{\rho_s}\right)^n E_{wall} \tag{4}$$

where E_{wall} is the matrix modulus in the cell walls as distinct from the matrix modulus in the interior of the cells, E_m (the anisotropy of the cell walls is not taken into account, but this is not expected to have significant consequences for a closed cell foam, for which stretching is the dominant mode of deformation of the cell walls[19]). In the case where $E_{wall} = E_m = 0.8$ MPa (the rubbery modulus of unmodified PS), taking $C = 1$ and $n = 1$, and for relatively small ϕ, equation (4) becomes

$$E = \left(1-\frac{\rho}{\rho_s}\right)E_m + \frac{1+2\frac{\rho_s}{\rho}\alpha\phi}{1-\frac{\rho_s}{\rho}\phi}\frac{\rho}{\rho_s}E_m \approx (1+2\alpha\phi)E_m \tag{5}$$

The predictions for the closed cell foam for a uniform matrix modulus are therefore close to the Halpin-Tsai predictions (cf. equation (2)). The foam model is hence

somewhat superfluous in descriptions of the glassy state, where, as discussed previously, classical micromechanical models are already able to account for the main trends in the data.[10,13] It follows that a possible interpretation of the behavior in the rubbery state is that $E_{wall} \neq E_m$. As shown in Figure 9, the foam model with $C = 1$ and $n = 1$ is roughly consistent with the data at large ϕ_L if E_{wall} is taken to be about 30 MPa, in qualitative agreement with the conclusions of earlier work, i.e. that the cell wall matrix modulus must be some 2 orders of magnitude greater than the rubbery modulus of unmodified PS for a foam model of this type to describe the data successfully.[10] A restriction in mobility of non-intercalated regions of the matrix is at least plausible in the laponite-rich regions that constitute the cell-walls in the cellular structures visible e.g. in Figure 2. The rms end-to-end distance associated with the entanglement molar mass, M_e, in PS, is approximately 6 nm, so that confinement to regions of space with similar or smaller dimensions, coupled with strong interactions with the confining substrates, as expected for both the PS and the acrylate in the presence of the PEO-based macromonomer, may lead to significant changes in elastic properties. On the other hand, E_{wall}, remains well below the glassy modulus, so that the corresponding polymer still undergoes a glass transition.

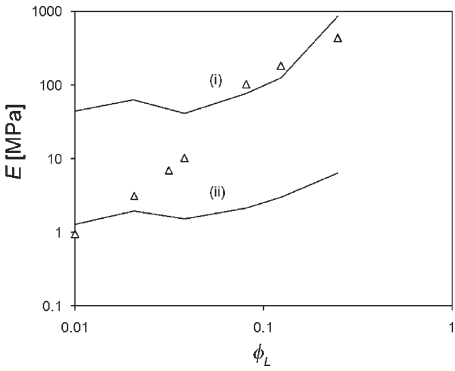

Figure 9.
Rubbery modulus of PS/laponite films at 160 °C as a function of ϕ_L, along with (i) predictions from equation (4) for $n = 1$ and $C = 1$ and $E_{wall} = 30$ MPa (see text), and (ii) predictions from equation (4) for $n = 1$ and $C = 1$ and $E_{wall} = 0.8$ MPa.

At low ϕ_L, the data were closer to the predictions of Halpin-Tsai or, equivalently, the foam model with $E_{wall} = E_m = 0.8$ MPa, also shown in Figure 9. Given that the effective laponite concentration in the cell walls decreased as the overall laponite concentration decreased, and the cellular structure was no longer well defined (e.g. for PS/5 wt% laponite in Figure 2(a)), it may be argued that confinement was no longer effective at these concentrations for any reasonable definition of the wall thickness (the predictions of equation (4) are relatively insensitive to the choice of cell wall thickness). Thus the steep increase in modulus at low ϕ_L may reflect a cross-over from a regime in which the aforementioned confinement effects are minor, to a regime in which they dominate the response of the films. This is believed to provide a more consistent interpretation than in previous work,[10] where a similar foam model was invoked to account for data from PS/laponite films with a more limited composition range (maximum nominal laponite content of 20 wt%). Even so, the interpretation depends on simple models for what are in reality highly complex systems, and even in the case of well-defined model cellular structures, the scaling behavior is not fully understood.[18] Moreover, at the highest laponite contents the rubbery plateau is poorly defined, the modulus falling off with temperature, possibly because of the structural changes discussed in the context of Figure 8, so that the values measured at 160 °C may not reflect the degree of reinforcement associated with the initial cellular arrangement. However, qualitatively at least, the results provide a strong indication of the importance of the local laponite concentration on mechanical properties via its influence on the local matrix properties. The relatively low degree of exfoliation encountered in the present systems at high laponite contents results in a reduced number of particles per unit volume when the particles are uniformly dispersed in the polymer matrix. However, the high local

particle concentrations that result from the latex route employed here are thought to be sufficient to result in significant changes in the global mechanical response. One might therefore speculate that if a uniform dispersion of highly exfoliated laponite could be obtained at a sufficiently high concentrations, the confinement effects invoked here would involve the whole of the matrix, again leading to much greater stiffness than predicted by classical models (indeed at upwards of about 50% by volume of laponite, most, if not all of the matrix would be expected to remain glassy on the basis of the present results, since the whole nanocomposite would be effectively intercalated). It is unlikely that such nanocomposites could be prepared and formed using conventional melt processing techniques so that the idea of producing a latex or a powder containing high concentrations of encapsulated exfoliated laponite (or a similar filler) remains of considerable interest.

Conclusion

Laponite contents of up to 50 wt% were achieved in both PS and acrylate films by the latex route, the laponite rich regions forming a continuous cellular structure at the highest laponite concentrations. In both cases, MDSC suggested the existence of a significant ''rigid amorphous fraction'' of the matrix at temperatures above T_g, which was argued to be associated with intercalation of the laponite stacks. However, the rigid amorphous fraction was argued to be insufficient to explain the large increases in stiffness above T_g with respect both to the unmodified matrices and the predictions of simple micromechanical models based on the assumption that the remainder of the matrix shows the same stiffness as the bulk polymer. The behavior above T_g was therefore accounted for in terms of a ''foam model'' involving two levels of matrix immobilization in the rubbery state: full immobilization in the interlayer galleries (the rigid amorphous fraction) and partial immobilization in the remainder of the matrix in the laponite-rich regions corresponding to the cell walls. Comparison of the cellular structure with a non-cellular structure produced by plane strain compression confirmed the importance of the cellular structure for obtaining high stiffness in the rubbery state in the present case.

Acknowledgements: This work was supported by the EU Project NAPOLEON and technical support was provided the Centre Interdisciplinaire de Microscopie Electronique (CIME) of the EPFL.

[1] N. Hasegawa, M. Kawasumi, M. Kato, A. Usuki, A. Okada, *J. Appl. Polym. Sci.* **1998**, *67*, 87.
[2] J. C. Halpin, J. L. Kardos, *Polym. Eng. & Sci.* **1976**, *16*, 344.
[3] T. Mori, K. Tanaka, *Acta Metallurgica* **1973**, *21*, 571.
[4] J. Cho, M. S. Joshi, C. T. Sun, *Compos. Sci. Tech.* **2006**, *66*, 1941.
[5] E. Reynaud, T. Jouen, C. Gautheir, G. Vigier, J. Varlet, *Polymer* **2001**, *42*, 8759.
[6] A. Lazzeri, Y. S. Thio, R. E. Cohen, *J. Appl. Polym. Sci.* **2004**, *91*, 925.
[7] Z. S. Petrovic, I. Javni, A. Waddon, G. Banhegyi, *J. Appl. Polym. Sci.* **2000**, *76*, 133.
[8] C. J. G. Plummer, M. Rodlert, J.-L. Bucaille, H. J. M. Grünbauer, J.-A. E. Månson, *Polymer* **2005**, *46*, 6543.
[9] M. Rodlert, C. J. G. Plummer, Y. Leterrier, J.-A. E. Månson, *J. Rheol.* **2004**, *48*, 1049.
[10] R. Ruggerone, C. J. G. Plummer, N. N. Herrera, E. Bourgeat-Lami, J.-A. E. Månson, *Eur. Polym. J.* **2009**, *45*, 621.
[11] E. Bourgeat-Lami, N. Negrete-Herrera, J.-L. Putaux, A. Perro, S. Reculusa, S. Ravaine, E. Duguet, *Macromol. Symp.* **2007**, *248*, 213.
[12] S. Reculusa, C. Poncet-Legrand, S. Ravaine, C. Mingotaud, E. Duguet, E. Bourgeat-Lami, *Chem Mater.* **2004**, *14*, 2354.
[13] R. Ruggerone, C. J. G. Plummer, N. N. Herrera, E. Bourgeat-Lami, J.-A. E. Månson, *Solid State Phenomena* **2009**, *30*, 151.
[14] H. Suzuki, J. Grebowicz, B. Wunderlich, *Makromol. Chem.* **1985**, *186*, 1109.
[15] C. Schick, A. Wurm, A. Mohamed, *Colloid. Polym. Sci.* **2001**, *279*, 800.
[16] J. Kim, M. M. Mok, R. W. Sandoval, D. J. Woo, J. M. Torkelson, *Macromolecules* **2006**, *39*, 6152.
[17] A. P. Roberts, E. J. Garboczi, *Acta Mater.* **2001**, *49*, 109.
[18] L. J. Gibson, M. F. Ashby, ''*Cellular Solids: Structure and Properties*'', Pergamon Press, Oxford **1988**.
[19] R. Ruggerone, C. J. G. Plummer, J.-A. E. Månson, *to be submitted.*

